

D.S. Hallgren and C.L. Hemenway  
Dudley Observatory and State University of New York at Albany,  
Albany, N.Y. USA

#### Abstract

Analysis of craters found on polished plates exposed during Skylab has provided data for a flux measurement over the mass range  $10^{-15}$  to  $10^{-7}$  gms. Chemical analysis of residues in the craters shows a high incidence of aluminium. A variety of morphological forms are described.

A major part of the S-149 experiment<sup>1</sup> on Skylab involved the study of impact craters on highly polished metal surfaces. Samples of polished copper, stainless steel, and silver were exposed in sets of four cassettes, each set having a polished plate sample area of  $0.06 \text{ m}^2$ . Each cassette is in two parts, a stationary half called the "pan" and a movable half called the "cover". During exposure the covers face in either the solar or anti-solar direction. Figure 1 illustrates the deployment of the S-149 experiment in the solar and anti-solar modes. The Z axis direction was highly stabilized with respect to the sun but the spacecraft underwent slow oscillation about Z. The pans, therefore, being parallel to the Z axis were not directed toward a fixed direction in space. Table 1 shows the exposure data for each of the three sets of cassettes which were returned. A fourth set of samples is currently being exposed awaiting a possible future return to Skylab.

Optical scanning is the principal method used for the detection of craters. All of the samples have been scanned at 200 X, and about 25 % have been re-examined at 500 X. In addition a small area (approx.  $63 \text{ mm}^2$ ) has been scanned in a scanning electron microscope at 5000 X. The optical scanning to date has revealed a total of 78 craters ranging in size from  $1.9 \mu$  inside diameter to  $135 \mu$  inside diameter. The small area studies in scanning microscope have shown six classic submicron craters as small as  $0.3 \mu$ . The fluxes computed from the data are shown in Figure 2.

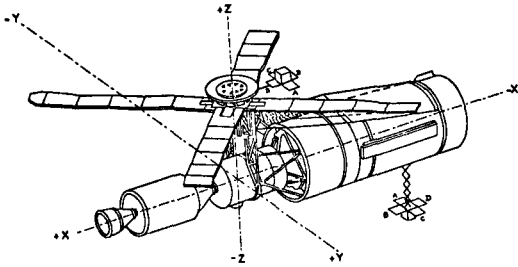


Figure 1  
Schematic of S-149 Deployment

Type	Deployed	Duration
Anti-solar (SL 2/3)	6/23/73	34 days
Solar (SL/3)	8/6/73	46 days
Solar (SL/4)	11/22/73	33 days
Solar SL/4+	2/3/74	260 days to date

Table 1  
Exposure Times

Due to the orientation of the collector, the region of space seen by the pans is the same for both the solar and anti-solar exposures while the covers point along a single axis. In each case the fluxes for the pans exceed those for the covers by a factor of 5 to 10. Note in Figure 2 that the fluxes computed from the submicron craters found in the scanning electron microscope are higher than those for the larger craters by a factor of about  $10^3$ .

All fluxes were computed using a crater-to-projectile diameter ratio of 3 which presumes all particles to have the same densities and impacting velocity. Shielding factors to correct for the field of view for each pan and cover were applied in the flux calculation; these are listed in Table 2.

In addition to the flux determination the craters have been examined in the

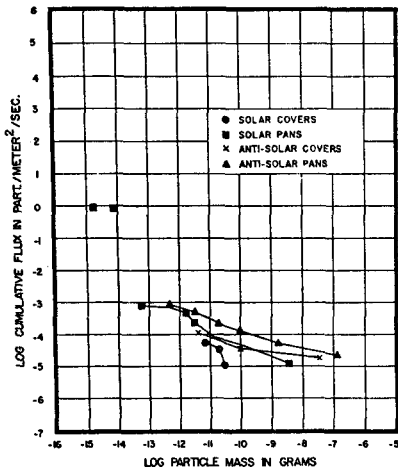


Figure 2  
Flux from Crater Data

Cassette Half	Solar	Anti-solar
Cover	52.8	56.3
Pan	40.9	43.6

Table 2  
Combined Shielding Factors (%)

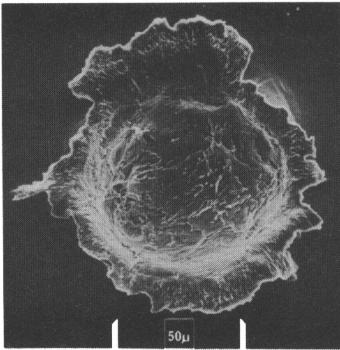
scanning electron microscope to study the variability in morphology of the crater interiors. This data has been computed with chemical analyses of the residues seen in the crater interior.

Figures 3 - 6 show representative examples of four general types of crater morphology observed on copper plates. In Figure 3 the crater interior shows distinct signs of melting. This type of structure was limited to the larger craters i.e. greater than  $20\ \mu$  inside diameter.

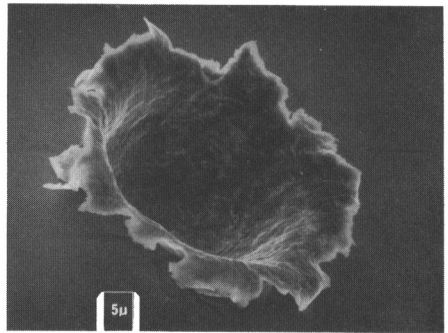
Figure 4 shows an example of the most prevalent structure. The term "textured" has been used to describe the generally rough interior.

Figure 5 shows one of three craters in which lumps of residue could be seen within the crater. The last type, shown in Figure 6, has no internal structural detail.

While it is apparent that the craters in Figure 5 and 6 show distinctly different interior structure we emphasize that the structures seen in Figures 3 and 4 are also



**Figure 3**  
Crater with Melted Interior



**Figure 4**  
Crater with Textured Interior

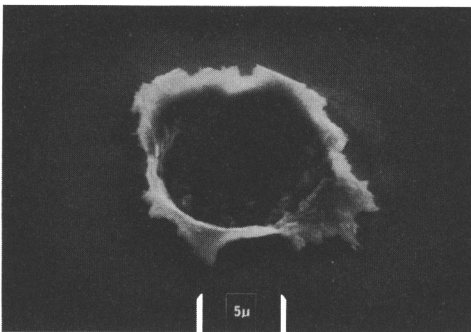


**Figure 5**  
Crater with Lumpy Structure  
or Residue

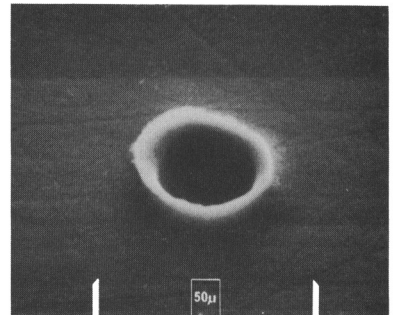


**Figure 6**  
Smooth Structureless Crater

sufficiently distinct to define crater types. Because of what looks like a sequence of potential physical relevance in these micrographs, attempts were made to correlate morphology with observed parameters such as crater diameter, crater depth and diameter to depth ratio; no systematic relationship could be established. It would appear that crater morphology may be related to other physical parameters involved in the collision such as the strength and structure of the original particle.

Chemical analysis of the interior walls and lips of the craters was carried out using an energy dispersive x-ray spectrometer in the scanning electron microscope for counting times of 100 - 1000 seconds. Even though there appear to be distinct types of craters as seen from the morphology no classification can be made on the basis of the residual elements from the impacting particle detected within the craters. Size alone does not determine the ability to detect residues: some craters one micron or less in diameter show residues while the largest crater analyzed showed no detectable residue even with long counting times (1000 sec.). As seen in Table 3, the element most frequently detected was aluminum and, in all, 10 different elements have been detected. Residues may be found exclusively on the lips of a crater, exclusively in the interior, or distributed over either but it is not possible to predict from the appearance of a crater alone where the residue will be found. About 55% of the impact craters yielded

Type	Dia ( $\mu$ )	Dia/depth	Elements						
<u>Smooth</u>									
B-1-12-2	5.2	4.3	Al						
C-2-9-9-2	1.8				Cr	Fe	Ni		
<u>Melted</u>									
B-1-12-1	47	2.1					Fe		
A-3-15-2	21	1.8	Al						
A-3-16-2	20	1.9	Al						
A-3-16-3	31	1.9	Al						
<u>Lumpy</u>									
B-1-12-4	15	3.9	Mg	Al	Si	S	K	Fe	Ca
B-2-9-3-1	1.8	-			Si	S	Zn		
B-3-15-9-1	12	2.6	Al						
<u>Textured</u>									
B-1-12-3	7.8	2.8	Mg		Si				
D-2-16-8-1	2.5	-		Al	Si				
A-3-15-1	7.8	3.0	Al						
B-3-13-1	6.9	2.5			Si	S		Fe	
C-3-14-1	5.6	3.1	Al						
C-3-14-2	5.4	3.6	Al						
C-3-14-4	4.9	4.1	Al						
C-3-14-5	6.5	3.3	Al						
C-3-16-1	2.1	-	Al	Si					

Table 3  
Elements Detected Within Craters

detectable residual elements.

It might be supposed that detection of many craters with aluminum residues indicates that the craters were produced by secondary impacts resulting from micrometeorites striking the spacecraft. There is a possibility of this happening during the solar exposure<sup>2</sup> but on the anti-solar exposure, where most of the aluminum containing craters were found, this is highly unlikely because the S-149 samples were out of the field of view of most of the spacecraft.

In summary the S-149 experiment has provided a long duration measurement of the micrometeorite flux in near-earth vicinity over the mass range  $10^{-15}$  to  $10^{-7}$  gm. Over this mass range the flux is observed to be greater by about an order of magnitude than those measured on the lunar surface. A sharp discontinuity is suggested in the flux at a mass of about  $10^{-13}$  gm. The fact that 70 out of the 78 craters found were on the pans indicates that most of the detected particles were in near circular heliocentric orbits. Examination of the crater interiors as seen in the scanning electron microscope indicates that there are considerable variations in the interior structures of the micrometeorite impact craters. Detection of residual elements from micrometeorites within the craters has been successful for craters even those as small as one micron. The most frequently detected element is aluminum which, considering meteoritic abundances, is quite surprising. Evidence for particle clustering has also been found.

#### References

1. C. L. Hemenway, D. S. Hallgren and C. D. Tackett, "Near-Earth Cosmic Dust Results from S-149", AIAA/AGU Conference on Scientific Experiments of Skylab, Huntsville, Alabama, 1974, AIAA Paper 74-1226, p. 7.
2. D. S. Hallgren, C. L. Hemenway and W. Radigan, "Micrometeorite Penetration Effects in Gold Foil", COSPAR, Varna, Bulgaria, 1975, Space Research XVI, in press.